

Article

Influence of the Distribution and Level of Post-Tensioning Force on the Punching Shear of Flat Slabs

Sarah S. Elsheshtawy ^{1,*}, Ata K. Shoeib ², Amal Hassanin ² and Dina M. Ors ¹¹ Faculty of Engineering and Technology, Future University in Egypt, Cairo 11835, Egypt² Faculty of Engineering El-Mattaria, Helwan University, Helwan 11795, Egypt

* Correspondence: sarah.elsheshtawy@fue.edu.eg

Abstract: Punching shear is the most common failure mechanism of slabs that are supported directly on columns. The slab–column connection is always vulnerable to critical punching shear; thus, it is necessary to investigate the effect of various parameters on the punching shear behavior of the flat slabs. This work presents an experimental study to evaluate the effect of the level of prestressing force and layout of the strands on the punching shear behavior of the slab–column connection in terms of the maximum load, deflection, stiffness, ductility, and the absorbed energy. Five square post-tension flat slabs (2000 mm × 2000 mm) with 150 mm thickness were tested. Increasing the prestressing force increased the maximum load and the ductility with a delay in damage in the case of uniformly distributed strands. Additionally, the banded layout of the post-tensioning strands significantly increased the punching shear capacity of the post-tensioned flat slabs at all levels of prestressing. The influence of the layout of the strands on the flat slab ductility is clearly visible in cases of high prestressing force as the ductility decreases in cases with distributed strands when compared to the same flat slabs with banded strands. Finally, the predicted values of the ultimate load of the punching shear using different codes, including the Egyptian Code of Practice (ECP-203), the American Building code (ACI-318), the CEB-FIP Model code and the Euro code, are compared to the experimental values of the ultimate punching shear strength of the post-tensioned and non-post-tensioned flat slabs.

Keywords: flat slab; punching shear; post-tensioning; strands layout; level of prestressing



Citation: Elsheshtawy, S.S.; Shoeib, A.K.; Hassanin, A.; Ors, D.M. Influence of the Distribution and Level of Post-Tensioning Force on the Punching Shear of Flat Slabs. *Designs* **2023**, *7*, 1. <https://doi.org/10.3390/designs7010001>

Academic Editors: Tiago Pinto Ribeiro and José António Correia

Received: 4 October 2022

Revised: 16 November 2022

Accepted: 2 December 2022

Published: 21 December 2022



Copyright: © 2022 by the authors. Licensee MDPI, Basel, Switzerland. This article is an open access article distributed under the terms and conditions of the Creative Commons Attribution (CC BY) license (<https://creativecommons.org/licenses/by/4.0/>).

1. Introduction and Background

Flat slab is one of the most common among the different types of reinforced concrete slabs that have been used in the last decades. This is due to the savings it offers in terms of the clear height that is used in commercial and residential buildings, the construction time and the flexibility it offers for architectural remodeling. One of the main concerns of flat slabs is the sudden local brittle punching shear failure that occurs due to the large stress localization at the column–slab joints and which leads to global flat slab failure. The most common methods to reduce the punching shear stress are to avoid the punching shear failure or to strengthen the flat slabs against the punching shear failure by decreasing the large load localization at column–slab joints. Flat slab with a PT system is an economical solution for when spans exceed the limits that can be covered with traditional flat slabs even when they are strengthened with drop panels, column heads or even increase slab thickness. Malvade et al., 2017 [1] designed post-tensioning flat slabs with different post-tensioning sequences using the SAFE software to model their resistance to earthquakes that carry gravity loads, lateral loads, and excessive bending moments. The model consisted of 8 m × 8 m two-way post-tensioned flat slabs with 200 mm thickness supported on four columns of size 400 mm × 400 mm. To avoid torsion in the slabs, the authors recommend the stretching of one tendon in X-direction then the stretching of another tendon in Y-direction and comparing this with the stretching of all tendons in one direction first then the stretching of all tendons in the other direction.

Mohammed et al., 2017 [2] investigated the effects of different parameters on the behavior of post-tensioned flat slabs. The area of post-tensioning tendons, the eccentricity of tendon profile, the jacking force in tendons, stress in steel tendons and the compressive strength of concrete were the main variables in their study. The authors found that optimizing the area of post-tensioning tendons reduces the cost.

Abd El-Mottaleb et al., 2018 [3] studied the effect of various parameters on the behavior of a two-way post-tensioned flat slab. The thickness of the flat slab, compressive strength of the concrete, the value of the jacking force, the area of strand and the effect of openings in the slab were the various parameters used to design the PT flat slabs. Their results showed that using post-tensioning cables produced a remarkable reduction in the deflection value of the flat slabs and that the bending moment is inversely proportional to the ratio of jacking force to the area of strand for larger thickness.

Töröka et al., 2018 [4] compared the required cost between normal reinforced concrete flat slabs and the post-tensioned flat slabs for spans equal to 7, 8 and 9 m using the same concrete compressive strength. The researchers also showed different uses for post-tensioned flat slabs, including as transfer plates that are mainly used to design ground floors with larger spans to increase commercial areas in public buildings. The researchers used Adapt Builder 2017 to design the slabs and to calculate the total cost. The researchers recommended the use of PT flat slabs rather than normal RC slabs as the PT flat slabs saved 10% to 20% of the required material quantities for a minimum 7-m span and a live load of 3 kN/m².

Töröka et al., 2019 [5] studied the possibility of using post-tensioning methods to design PT flat slabs for many buildings. The researchers recommended using post-tensioning flat slabs in cases where spans were greater than seven meters, and especially in cases of the existence of voids within slab areas of limited dimensions due to different design codes. Although many countries use post-tensioning flat slabs widely, some countries, such as Romania, avoid the usage of this method because of the difficulty of its design. Therefore, more research is required to facilitate an understanding of the behavior of post-tensioning flat slabs for design requirements.

Binh et al., 2022 [6] studied the effect of a joint made of unbonded post-tensioned concrete. The experimental program consisted of six large-scale specimens, three connections of UPC–CFT column, two connections of RC slab–CFT column and one conventional connection of UPC–RC column (control specimen). Their results show that using UPC slab–CFT column connections increased punching shear resistance, deformation capacity, ductility, and the absorbed energy index when compared with UPC slab–RC connection. Using prestressing tendons rather than RC slab–CFT column specimens increased the punching shear resistance, and enhanced the cracking resistance, pre-cracking stiffness and post-cracking resistance.

This study presents the experimental work that was performed to investigate the effect of various parameters on the level of prestressing and the layout of cables on the punching shear behavior of post-tensioning flat slabs.

2. Experimental Program

The experimental program of this study includes five square flat slab interior column connections. All specimens had the same dimensions of 2000 mm × 2000 mm in plan with a thickness 150 mm and with top and bottom reinforcement meshes of 5 Φ 10/m. The main variables were the level of prestressing and the strands layout. NF is the control specimen of non-prestressed flat slab. C2PS and C3PS are two post-tensioned flat slabs with cables banded under the loading plate but with different level of prestressing (two and three strands, respectively). D2PS and D3PS are two post-tensioned flat slabs with strands spaced by 0.67 m and centered by a loading plate but with different level of prestressing (two and three strands, respectively). Figure 1 and Table 1 indicate details of all tested specimens of the experimental program.

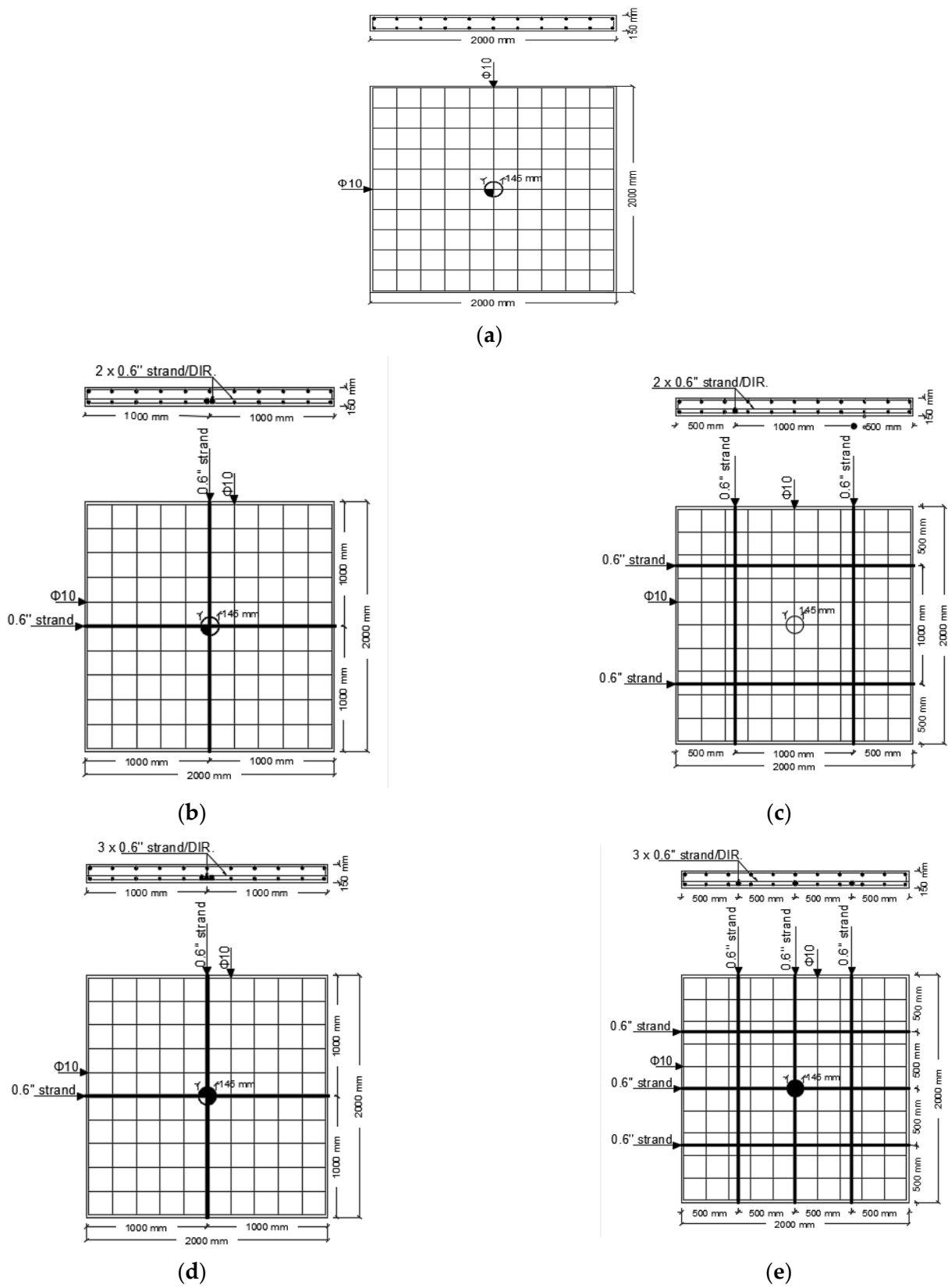


Figure 1. Details of tested specimens. (a) Control specimens (NF); (b) post-tension with two cables, central space (C2PS); (c) post-tension with two cables, 67 mm space (D2PS); (d) post-tension with three cables, central space (C3PS); and (e) post-tension with two cables, 500 mm space (D3PS).

Table 1. Dimensions and properties of reinforced concrete, steel reinforcement and post-tensioning cables.

Specimen ID	Concrete Dimensions		Mild RFT			Prestressing System				
	Plan m × m	Thickness mm	f_{cu} MPa	Top and Bottom Reinforcement	Cover mm	f_y MPa	No. of Strands	Alignment	f_y MPa	Cover mm
NF	2 × 2	150	44.50	5 Φ 10/m	20	500	—	—	—	—
C2PS							2 Φ 0.6"/direction	Banded	—	
C3PS							3 Φ 0.6"/direction	Banded	—	
D2PS							2 Φ 0.6"/direction	Distributed	1640	
D3PS							3 Φ 0.6"/direction	Distributed	40	

3. Material Properties

The materials used in the fabrication of all tested specimens are the local available materials and the same common traditional method of casting is used for all tested slabs. The concrete mix was designed to achieve 40 MPa. The mix consists of ordinary Portland cement, coarse aggregate, and fine aggregate with ratio of 1:3.5:1.8 by weight, respectively. The water-to-cement ratio was 0.55 and the cement content was 400 kg/m³.

Additives were added to increase the workability of concrete. R2004-SILKA is a highly effective plasticizer with a set-retarding effect for the production of free-flowing concrete in hot weather.

The characteristic strength of concrete was assigned by testing standard cubes with dimensions of 150 mm × 150 mm × 150 mm after 28 days of casting and in the test day the concrete average compressive strength achieved 44.5 MPa. The yield strength of the main reinforcement steel is 500 MPa according to the manufacturer. The yield and ultimate strength of the high strength cable with post-tensioning strands according to the manufacturer are 1640 MPa and 1860 MPa, respectively, and were tensioned by 200 kN. Table 2 summarizes all materials characteristics.

Table 2. Material characteristics of tested flat slabs.

Concrete				Mild Steel Reinforcement		Prestressing Cables		
Concrete Mix Proportion of 1 m ³				Design Cube Compressive Strength (MPa)	Test Day Cube Compressive Strength (MPa)	f_y (MPa)	f_y (MPa)	f_u (MPa)
Cement (kg)	Fine Aggregate (kg)	Coarse Aggregate (kg)	W/C					
400	1400	720	0.55	40	44.50	500	1640	1860

4. Test Set-Up and Loading Protocol

A typical punching shear test set-up was prepared for each tested flat slab. The flat slabs were supported by four I-beams spaced by 1.80 m center to center. Tested flat slabs were subjected to concentric incremental static load. The vertical load was applied by a 600-kN capacity jack fixed to the girder of a double A-frame that was made available at the RC laboratory in the Housing and Building National Research Centre (HBRC). The test set up is shown in Figure 2. The column was presented as circular steel plate with diameter 145 mm and 30 mm thickness. Strain gauges were installed to reinforcement bars and the post-tensioning cables. For PT cables, the strain gauges were installed at the midspan of each cable in each direction. Meanwhile, for the lower reinforcement mesh, the strain gauges were installed at the midspan of one rebar in each direction as shown in Figure 3. The deflection of tested specimens was detected using linear variable differential transformers (LVDT) which were installed in the mid shear span of each specimen, while two of them were installed under the circular steel plate as shown in Figure 4.



Figure 2. Test set-up for all tested specimens.

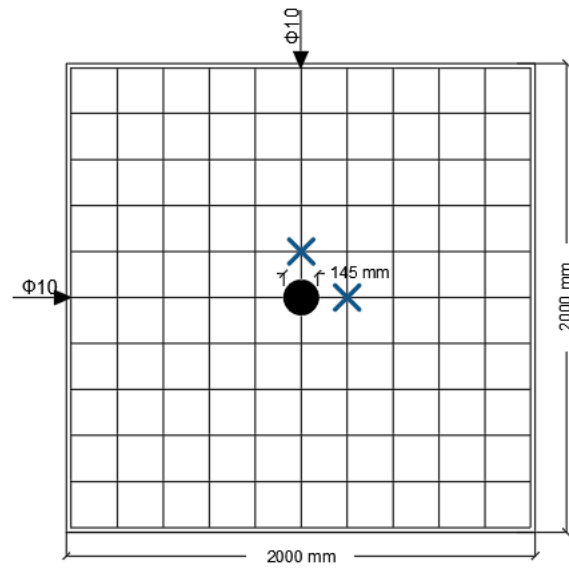


Figure 3. Position of strain gauges on the bottom reinforcement mesh.

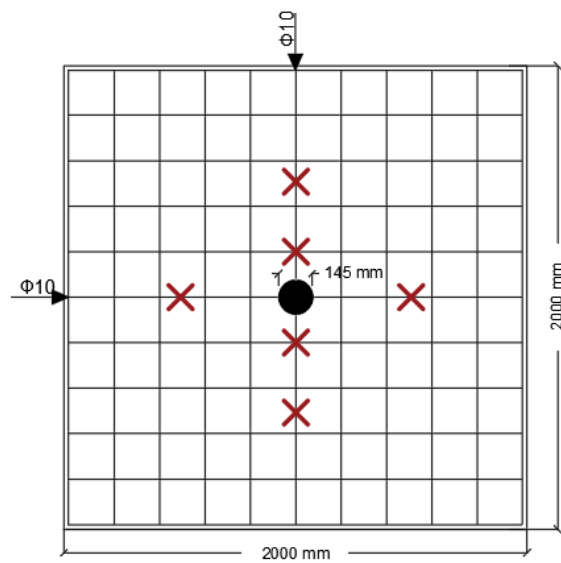


Figure 4. Position of LVDTs.

5. Test Results and Discussion

This section presents the experimental results of all tested flat-slab specimens. The main variables are the number and the alignment of the post-tensioning strands as banded or distributed in both directions. The specimens were tested under a concentric compressive load from a circular column with a diameter equal to 145 mm until failure. NF flat slab is the control non-prestressed specimen. C2PS and C3PS specimens are post-tensioned reinforced concrete flat slabs with bonded banded strands of 0.6", the difference is the level of prestressing, as two and three strands were applied for each slab, respectively. D2PS and D3PS specimens are post-tensioned reinforced concrete flat slabs with bonded distributed strands of 0.6", the difference is the level of prestressing as two and three strands were applied for each slab, respectively. The flat slabs were monitored during test until failure and the measured behavior is discussed in this section in terms of failure mode, load–deflection response, strain in mild steel, stiffness, ductility and absorbed energy.

5.1. Failure Modes

All tested specimens have the same dimensions and were tested until failure. The crack pattern was tracked until the formation of a major crack from the punching cone on the bottom surface of the tested flat slabs. The cracking load is significantly increased in the case of post-tension slabs—by 135.5%, 172%, 136.4% and 175% in case of C2PS, C3PS, D2PS and D3PS flat slabs, respectively—when compared with the control specimen (NF). The corresponding deflection of the cracking load is increased by 165%, 215%, 246%, and 224% in the cases of C2PS, C3PS, D2PS and D3PS flat slabs, respectively, when compared with the control specimen (NF).

The failure was represented by a clear brittle punching shear of all tested specimens as shown in Figure 5. The average punching cone diameter of post-tensioned slabs was larger than the control slab. In case of banded strands, the average punching cone diameter was larger than the specimens with distributed strands in either the case of two or of three strands. In case of a higher level of post-tensioning (PT), the average punching cone diameter was larger than the specimens with a lower level of post-tensioning (PT), for both banded and distributed strands. Table 3 presents the average punching cone diameter and failure type of all tested specimens. By increasing the maximum loads of tested specimens, the cone diameter increased.

Table 3. Average cone diameter and failure type for all tested specimens.

Specimen ID	P _{max} (kN)	Failure Mechanism	Average Cone Diameter (mm)
NF	197.5	Punching	65
C2PS	325	Punching	135
C3PS	293	Punching	115
D2PS	270	Punching	90
D3PS	278.5	Punching	97



Figure 5. Failure mode of all tested specimens.

5.2. Load–Deflection Response

The load–deflection response was measured during testing. The cracking and ultimate loads are presented in Table 4 as well as the corresponding average deflection under the loading plate edges. The cracking load was significantly increased in the case of PT slabs by 135.5%, 172%, 136.4% and 175.14% in the cases of C2PS, C3PS, D2PS and D3PS flat slabs, respectively, when compared with the control specimen NF. The corresponding maximum

deflections were reduced by 64.9%, 114.86%, 145.54% and 123.85% in the cases of C2PS, C3PS, D2PS and D3PS flat slabs, respectively, when compared with the control specimen NF. Figure 6 presents the load–deflection curve of all tested specimens NF, C2PS, C3PS, D2PS and D3PS. The control specimen NF failed at a maximum load of 197.5 kN with a corresponding deflection of 18.7 mm. Enhancing the normal reinforced concrete flat slab with post-tensioning cables increased the punching shear capacity of the tested specimens. The ultimate load of the C2PS, C3PS, D2PS and D3PS specimens increased by 64.6%, 48.4%, 36.71% and 41%, respectively, when compared with the control specimen NF. Considering the alignment of strands, specimens with banded strands (C2PS, C3PS) failed at a higher ultimate load than specimens with distributed strands (D2PS, D3PS) in case of two or of three strands. Considering the level of prestressing, the specimen with three strands (D3PS) failed at a slightly higher load than the specimen with two strands (D2PS) in the case of distributed strands. However, in the case of banded strands, the specimen with two strands (C2PS) failed at a higher load than the specimen with three strands (C3PS). The ultimate deflection of C2PS, C3PS, D2PS and D3PS specimens decreased by 17.11%, 45.5%, 14.97% and 22.5%, respectively, when compared with the control specimen NF. Considering the alignment of strands, the specimens with banded strands (C2PS, C3PS) had lower deflection values than the specimens with distributed strands (D2PS, D3PS) in the case of two or of three strands. Meanwhile, for the level of prestressing, the specimens with a higher number of strands (C3PS, D3PS) had lower deflection values than the specimens with lower number of strands (C2PS, D2PS) in case of banded or of distributed strands. Figure 6 and Table 4 summarize the load–deflection response of all tested flat slabs. The deflection was measured at two points under column edges, mid-spans and at supports using LVDTs. At ultimate load of each tested flat slab, Figure 7 shows that the deflection increases gradually along the slabs span from the support lines to the punching cone zone which achieves very large deflection values when compared to the same values along the span of the flat slabs.

Table 4. Load and deflection at ultimate point and cracking point.

Specimen ID	Ultimate				Cracking			
	Load		Deflection		Load		Deflection	
	P_{max} (kN)	$\frac{P_{slab}-P_{NF}}{P_{NF}} \times 100\%$	Δu (mm)	$\frac{\Delta_{slab}-\Delta_{NF}}{\Delta_{NF}} \times 100\%$	P_{cr} (kN)	$\frac{P_{slab}-P_{NF}}{P_{NF}} \times 100\%$	Δcr (mm)	$\frac{\Delta_{slab}-\Delta_{NF}}{\Delta_{NF}} \times 100\%$
NF	197.5	-	18.7	-	55.5	-	1.568	-
C2PS	325	64.6	15.5	17.11	130.7	135.5	2.586	64.9
C3PS	293	48.4	10.2	45.5	151.0	172	3.369	114.86
D2PS	270	36.71	15.9	14.97	131.2	136.4	3.85	145.54
D3PS	278.5	41	14.5	22.5	152.7	175.14	3.51	123.85

5.3. Strains in Mild Steel

Strain gauges were installed on the bottom steel reinforcement under the column faces to detect the strain of reinforcement rebar in each direction. Figure 8 presents the measured strains during loading. Some strain gauges were cut during construction of the specimens as in NF and C3PS specimens, while some strain gauges were cut before reaching the maximum load, as in the NF, D2PS and D3PS specimens. Some of these did not reach the yield strain which means that the failure mechanism is clearly a punching shear failure as in the C3PS specimen and in the C2PS, D2PS and D3PS specimens the measured strain exceeded the yield strain. This can be explained as being due to way these strain gauges were located at the perimeter of the punching shear cone and yielded due to the resistance of the splitting forces perpendicular to the compressive struts that extended from the loading plate through the slab depth until the formation of punching cone failure at the slab bottom reinforcement as shown in Figure 9 [7].

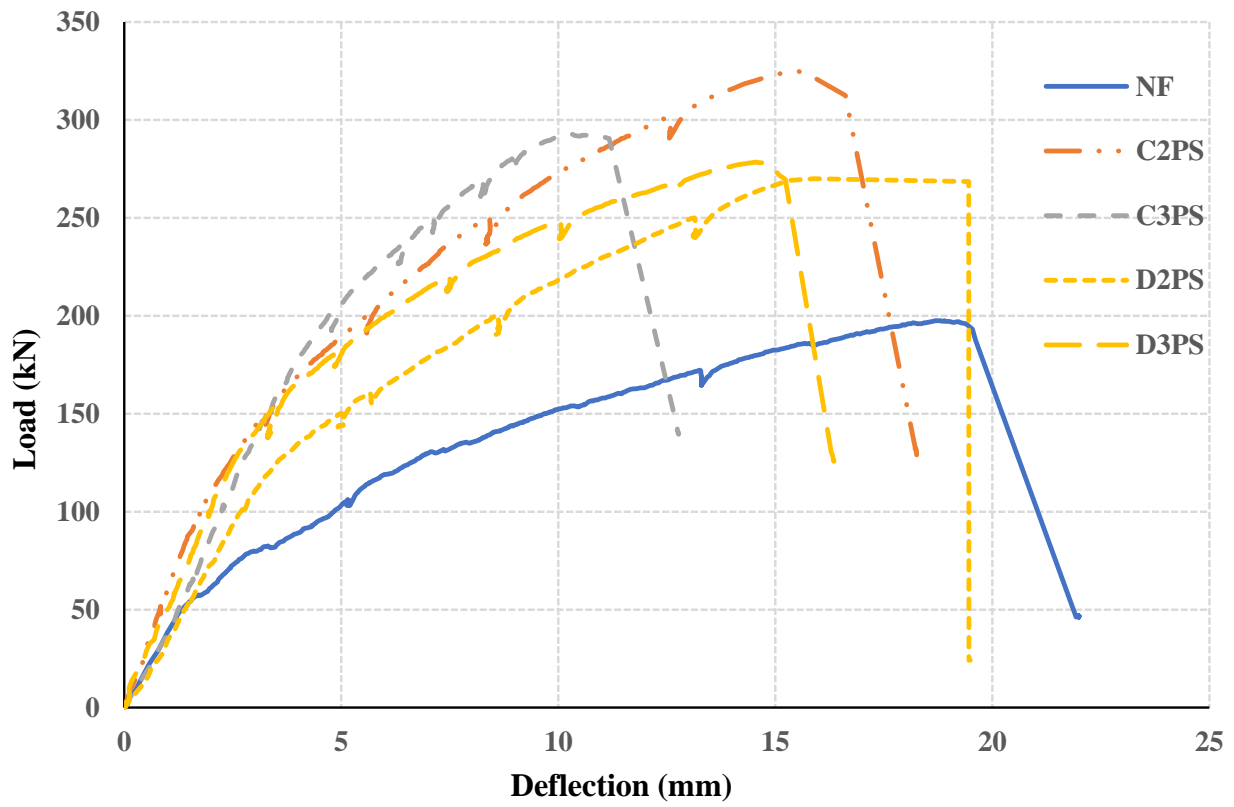


Figure 6. Load–deflection response of all tested specimens.

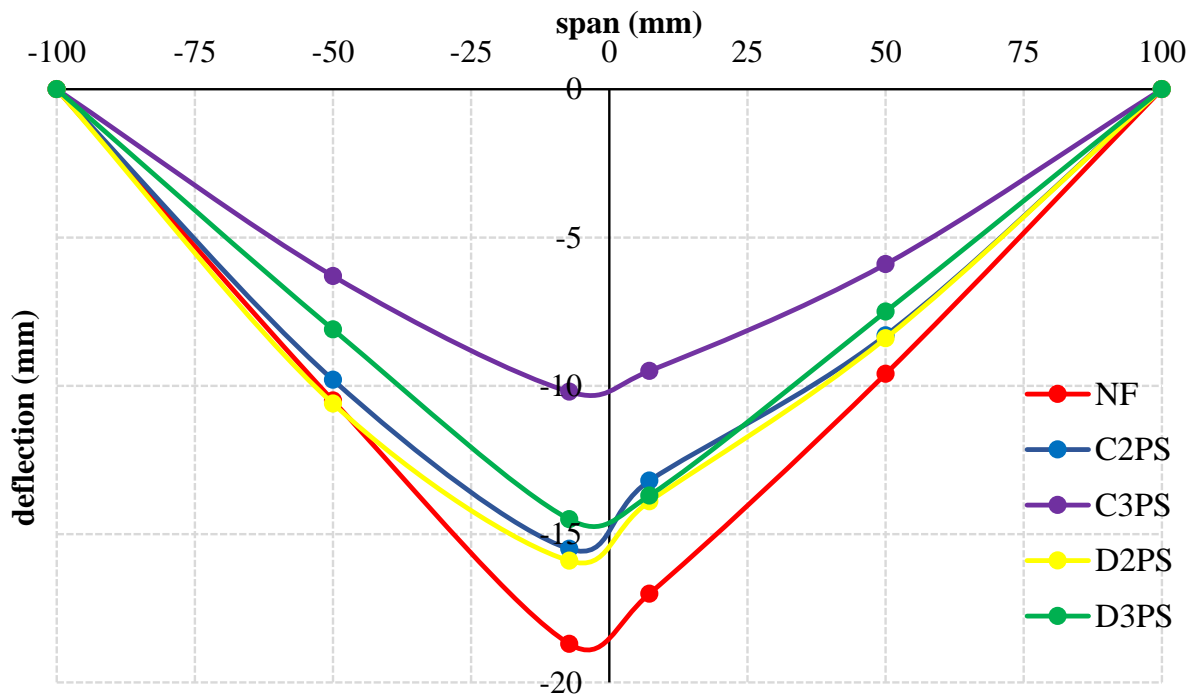


Figure 7. Deflection along specimens span at point of maximum load.

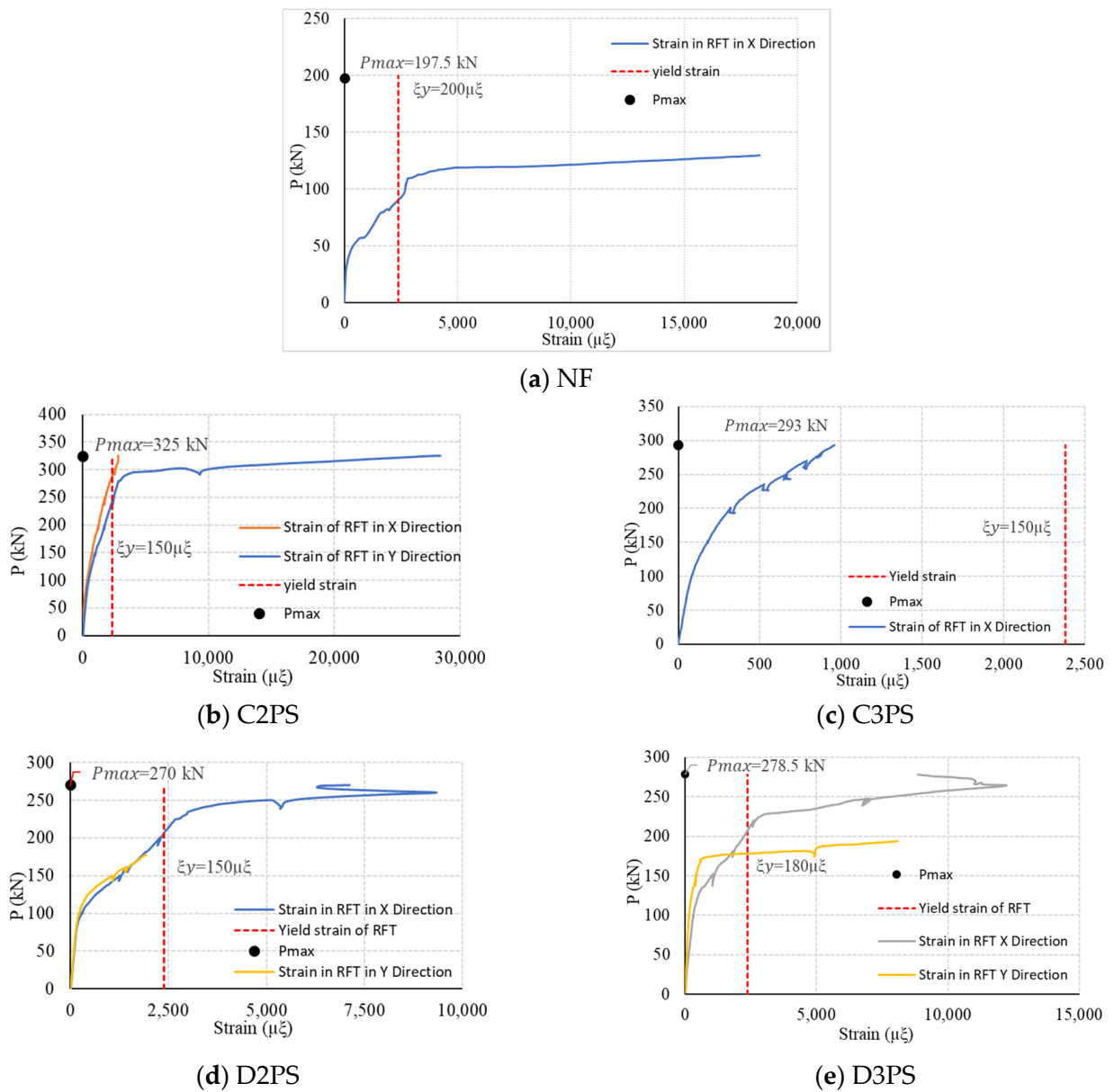


Figure 8. Load–strain response of steel reinforcement.

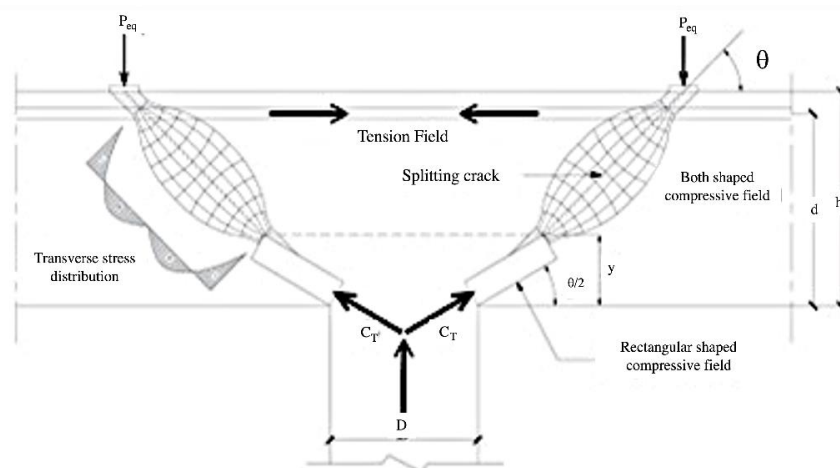


Figure 9. Force trajectories in punching cone zone.

5.4. Stiffness

Stiffness of the flat slabs is one of the most important parameters that can differentiate between non-post-tensioned flat slabs and post-tensioned flat slabs with different level of prestressing and lay out of strands. The initial stiffness is the slope of the load–deflection curve from zero point until the cracking point. The non-linear measured behavior of the flat slabs is approximated into two tangents after point of cracking, then the average slope of post-cracking tangents is the post-cracking stiffness of all tested flat slabs as shown in Figure 10. Post-tensioned flat slabs have larger initial stiffnesses of 50,541.38 kN/m, 44,820.42 kN/m, 34,077.92 kN/m, and 43,504.27 kN/m while the control specimen exhibited 35,394.41 kN/m. Post-tensioning of flat slabs significantly increased the post-cracking stiffness. The post-tensioned flat slabs achieved 15,059.68 kN/m, 21,216.2 kN/m, 11,533.99 kN/m, and 11,411.47 kN/m while the non-prestressed flat slab exhibited 8194.83 kN/m. Flat slabs with banded strands achieved higher stiffnesses of 15,059.68 kN/m and 21,216.2 kN/m than the specimens with distributed strands, which had stiffnesses 11,533.99 kN/m and 11,411.47 kN/m in the cases of two and three strands, respectively. In the case of banded strands, flat slab C3PS with a higher PT level had a larger stiffness, of 21,216.2 kN/m, than the same specimen C2PS with a lower level of prestressing, which had a stiffness of 15,059.68 kN/m. In the case of distributed strands, flat slab D2PS with a lower level of PT level had a slightly larger stiffness of 11,533.99 kN/m than the same specimen D3PS with higher level of PT level, which had a stiffness of 11,411.47 kN/m. Table 5 summarizes the stiffness of all tested specimens at all stages of loading and Figure 11 compares the stiffness of all tested flat slabs [8].

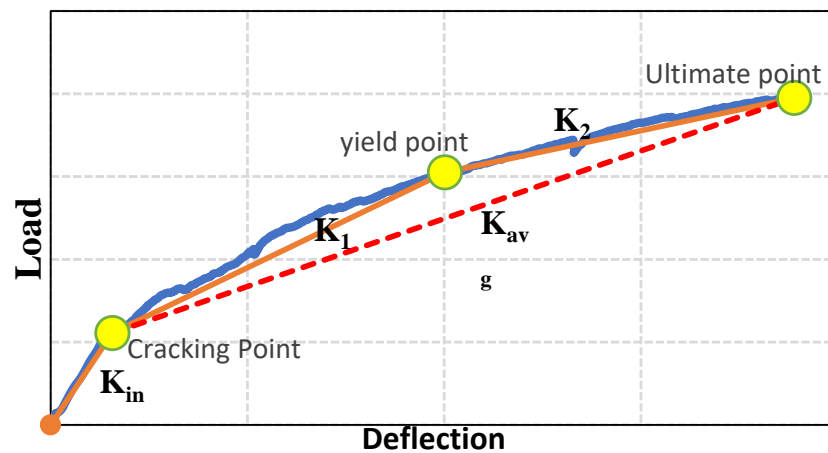


Figure 10. Initial and average stiffness for tested specimens.

Table 5. Stiffness for tested specimens.

Specimen ID	$K_{initial}$ (kN/m)	K_1 (kN/m)	K_2 (kN/m)	K_{avg} (kN/m)
NF	35,395.41	11,480.6	5068.14	8194.83
C2PS	50,541.38	19,929.1	10,134.1	15,059.68
C3PS	44,820.42	29,969.7	15,528.7	21,216.2
D2PS	34,077.92	14,625.1	9027.99	11,533.99
D3PS	43,504.27	15,124.6	6457.76	11,411.47

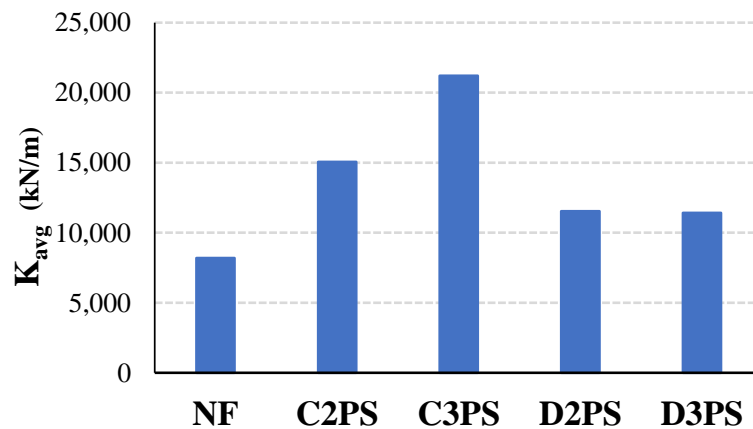


Figure 11. Average stiffness of tested specimens.

5.5. Ductility

Ductility (μ) of all tested flat slabs was calculated as the ratio between the maximum deflection at the ultimate load and the deflection at yield point ($\mu = \Delta u / \Delta y$) as listed in Table 6. The yield point is the point at which the slab stiffness decreases until it reaches its ultimate point, as shown in Figure 10. The NF exhibited the largest ductility of 1.89 followed by slabs with low level of prestressing of C2PS and D2PS. The least ductility was achieved by the slabs with a higher level of prestressing, C3PS and D3PS. The decrease of a slab’s ductility in case of prestressing is attributed to the decrease in the slab deflection at the same loading levels when compared with the normal flat slab without prestressing. Additionally, the increase of the level of prestressing enhances the slab stiffness, which leads to limited deformation and a decrease of the slab’s ductility. Figure 12 compares the calculated values of the ductility for all tested slabs [8].

Table 6. Ductility ratio for tested specimens.

Specimen ID	Δy (mm)	Δu (mm)	$\mu = \frac{\Delta u}{\Delta y}$
NF	10.017	18.896	1.89
C2PS	9.074	15.488	1.70
C3PS	6.005	10.062	1.67
D2PS	9.238	15.884	1.72
D3PS	9.811	14.534	1.48

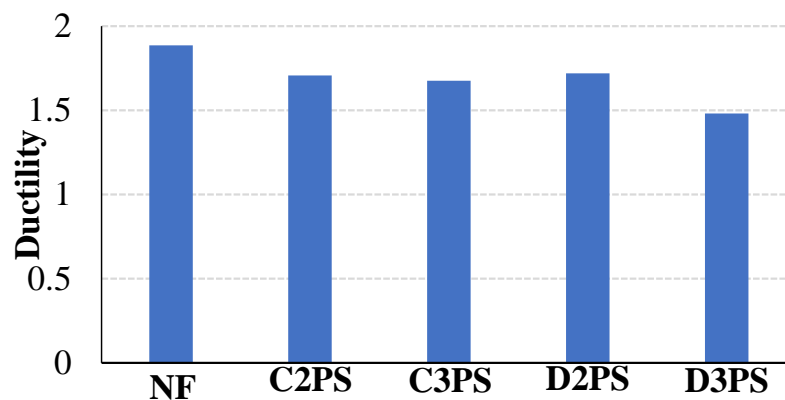


Figure 12. Ductility ratio for specimens.

5.6. Energy Absorbed

The damage exhibited by all tested flat slabs can be represented by the absorbed energy index (AEI). The AEI can be calculated as the ratio between the total area under a

load–deflection curve to the area under the elastic part only, as shown in Figure 13. The area under the elastic part (A_1) is calculated as the area under the curve until the appearance of the first crack. The total area under load–deflection curve (A_{total}) represents the toughness of the flat slab. The calculated values of the absorbed energy index (AEI) are listed in Table 7. The energy absorbed by the post-tensioned slabs in elastic part (A_1) is higher than the absorbed energy absorbed by the non-prestressed slabs. Thus, slabs with high post-tensioning level—C3PS, D3PS—achieved less AEI than the same flat slabs with low post-tensioning level—C2PS, D2PS—in alignments of both banded and distributed strands as shown in Figure 14 [8].

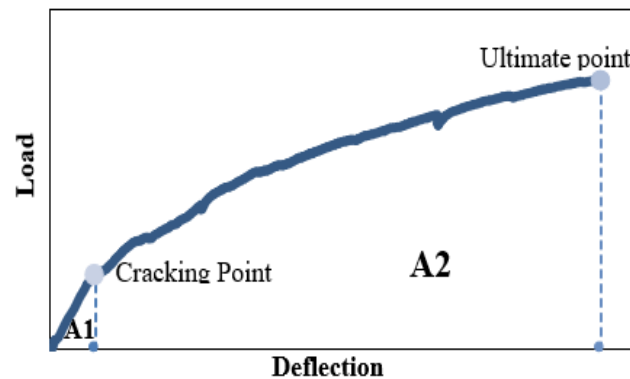


Figure 13. Area under the curve [8].

Table 7. Absorbed energy index for all tested specimens.

Specimen ID	A_1 (kN.m)	A_{total} (kN.m)	$AEI = \frac{A_{total}}{A_1}$
NF	4351	247,603	56.9
C2PS	16,899	331,252	19.6
C3PS	25,436	181,742	7.15
D2PS	25,256	276,679	10.95
D3PS	26,798	277,372	10.35

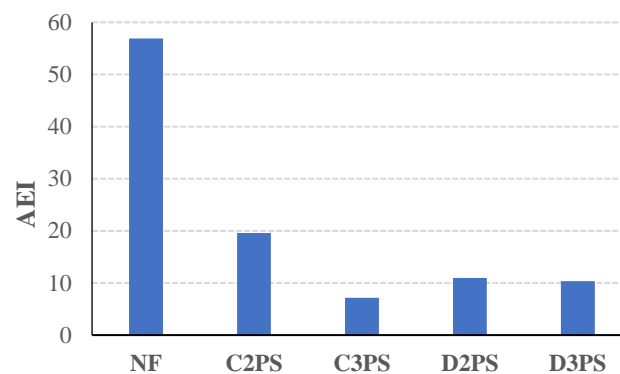


Figure 14. Absorbed energy index for tested specimens.

6. Design Codes

In this section different design code provisions are presented for both conventional non-prestressed reinforced concrete flat slabs and the prestressed flat slabs. Table 8 summarizes the punching shear strength of both post-tensioned and non-post-tensioned reinforced concrete flat slabs according to the ECP, ACI, CEB and EC. Additionally, Figure 15 presents a comparison between different code values for each slab with the experimental test results. This was conducted to investigate the different accuracies of each code when predicting the ultimate punching shear strength.

Table 8. Calculated P from different codes and the percentage between P_{code} and P_{actual} from experimental lab.

Specimen ID	$P_{exp.}$ (kN)	P_{code} (kN)				$P_{code} / P_{exp.}$			
		ECP	ACI	CEB	EC	ECP	ACI	CEB	EC
NF	197.5	191	230.3	259	279.4	0.97	1.17	1.30	1.40
C2PS	325	247.3	476	388.7	316	0.76	1.46	1.19	0.97
C3PS	293	269.8	498.6	388.7	334	0.93	1.70	1.33	1.14
D2PS	270	247.3	476	388.7	316	0.92	1.76	1.44	1.17
D3PS	278.5	269.8	498.6	388.7	334	0.97	1.79	1.40	1.19

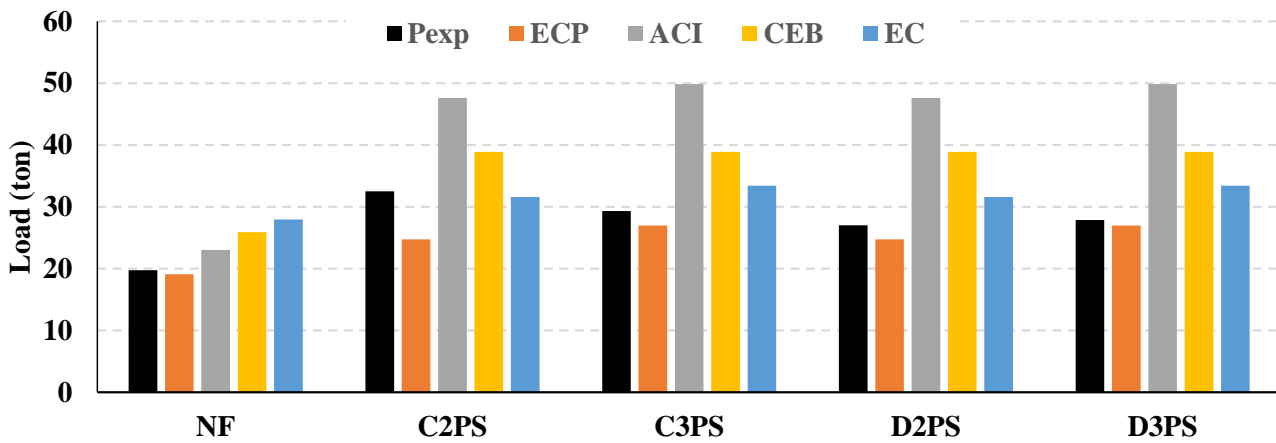


Figure 15. Comparison between codes ultimate punching shear strength of all specimens.

6.1. The Egyptian Code of Practice (ECP-203)

6.1.1. Non-Prestressed Reinforced Concrete Flat Slab

The Egyptian code of practice [9] assumes a failure surface at half the slab’s depth away from the column edges and the maximum flat slab shear strength is calculated using the minimum value calculated using Equation (1). The ultimate shear strength of the experimentally tested flat slab NF was calculated using Equation (1) and was compared to the experimental results, as shown in Table 8.

$$V_c(\text{MPa}) = \min \left\{ \begin{array}{l} 0.8 \left(\frac{\alpha \cdot d}{b_0} + 0.20 \right) \cdot \sqrt{\frac{f_{cu}}{\gamma_c}} \\ 0.316 \left(0.50 + \frac{a}{b} \right) \cdot \sqrt{\frac{f_{cu}}{\gamma_c}} \\ 0.316 \sqrt{\frac{f_{cu}}{\gamma_c}} \\ 1.70 \end{array} \right\} \cdot b_0 \cdot d \quad (1)$$

where $\alpha = 4, 3, 2$ for interior, edge, and corner columns, respectively; d is slab thickness; f_{cu} is concrete characteristic compressive strength; b_0 is perimeter of critical section of punching; and a and b are the short and long dimensions of column dimensions, respectively.

6.1.2. Post-Tensioned Reinforced Concrete Flat Slab

The Egyptian code of practice considers the effect of the post-tension in terms of the increase of the concrete’s compressive strength as well as the vertical force that supports the punching cone if the strands are inclined with the critical punching section zone. Equation (2) presents the ultimate punching shear force calculated using the Egyptian code of practice (ECP). The ultimate shear strength of the experimentally tested flat slabs

C2PS, C3PS, D2PS, D3PS were calculated using Equation (2) and were compared to the experimental results as shown in Table 8.

$$V_C = (0.27\sqrt{f_{cu}} + 0.30f_{p.c.})b_0d + V_p \tag{2}$$

where f_{cu} is the concrete characteristic compressive strength; $f_{p.c.}$ is the prestress; b_0 is the perimeter of the critical punching section; d is the slab depth; and V_p is the vertical component of prestress in tendon at supports.

6.2. The American Building Code (ACI-318) [10]

6.2.1. Non-Prestressed Reinforced Concrete Flat Slab

The American Concrete Institute (ACI) predicts the critical punching shear perimeter at half the slab’s depth away from the column edges and the ultimate flat slab shear strength was calculated using Equation (3). The ultimate shear strength of the experimentally tested flat slab NF was calculated using Equation (3) and compared to the experimental results as shown in Table 8.

$$V_c(\text{MPa}) = \text{the min of } \left\{ \begin{array}{l} \frac{1}{6} \left[1 + \frac{2}{\beta_c} \right] \lambda_s \sqrt{f'_c} \cdot b_0 d \quad \beta_c = \frac{\text{long column side}}{\text{short column side}} \geq 2 \\ \frac{1}{12} \left[\frac{\alpha_s d}{b_0} + 2 \right] \lambda_s \sqrt{f'_c} \cdot b_0 d \quad \alpha_s = 40 \text{ for interior columns} \\ \frac{1}{3} \lambda_s \sqrt{f'_c} \cdot b_0 d \end{array} \right\} \tag{3}$$

where V_c is the two-way shear strength of a normal weight flat slab without shear reinforcement; β_c is the column aspect ratio (long side/short side); λ_s is the size effect factor; f'_c is the concrete cylinder compressive strength = 0.85 f_{cu} and does not exceed 68 MPa; b_0 is the perimeter of the critical section; d is the effective slab depth; and α_s is 40, 30, 20 for interior, edge and corner columns, respectively.

6.2.2. Post-Tensioned Reinforced Concrete Flat Slab

Egyptian code of practice considers the effect of the post-tension in terms of the increase of the concrete compressive strength as well as the vertical force that supports the punching cone if the strands are inclined within the punching critical section zone. Equation (4) presents the ultimate punching shear force calculated using the ACI. The ultimate shear strength of the experimentally tested flat slabs C2PS, C3PS, D2PS, D3PS were calculated using Equation (4) and compared to the experimental results as shown in Table 8.

$$V_C = (\beta_p \sqrt{f_{cu}} + 0.30f_{p.c.})b_0d + V_p \tag{4}$$

where β_p is the smaller of 3.50 or $0.083(\frac{\alpha_s d}{b_0} + 1.50)$; f_{cu} is the concrete cylinder compressive strength; $f_{p.c.}$ is the mean effective prestress; and V_p is the vertical component of the prestress in the tendon passing through the critical section.

6.3. CEB–FIP Model Code [11]

6.3.1. Non-Prestressed Reinforced Concrete Flat Slab

The CEB–FIP model code calculates the maximum punching load carried by the flat slab assuming the polar symmetrical dispersion of the load using Equation (5). The failure surface is taken as three-times the distance of the slab’s depth away from the column faces. The ultimate shear strength of the experimentally tested flat slab NF was calculated using Equation (5) and compared to the experimental results, as shown in Table 8.

$$V_c = 0.12 \lambda_s (100\rho f_{cu})^{\frac{1}{3}} b_0 d \tag{5}$$

$$\lambda_s = 1 + \sqrt{\frac{200}{d}} \leq 2.00$$

$$\rho = \sqrt{\rho_x \cdot \rho_y} \leq 0.02$$

where λ_s is the coefficient of size effect; b_0 is the perimeter of the critical section; f_{cu} is the concrete characteristic compressive strength, which does not exceed 80 MPa; and V_c is the ultimate punching load capacity.

6.3.2. Post-Tensioned Reinforced Concrete Flat Slab

To enhance the ductility of the flat slabs, especially in the case of the high effect of the local brittle failure of the punching shear, the CEB–FIP model code-1990 treats the prestressing force as external applied compressive load if the tendons pass through the critical section. The prestress effect can be added to the previous Equation developed for the non-prestressed flat slabs as an excess of the ultimate punching shear forces as expressed in Equation (6). The ultimate shear strength of the experimentally tested flat slabs C2PS, C3PS, D2PS, D3PS were calculated using Equation (6) and compared to the experimental results as shown in Table 8.

$$V_c = 0.18 \lambda_s (100 \rho f_{cu})^{\frac{1}{3}} b_0 d + V_p \tag{6}$$

6.4. Euro Code [12]

6.4.1. Non-Prestressed Reinforced Concrete Flat Slab

Based on the Equations given by the CEB–FIP model code 1990; the euro code gives a similar equation and predicts the punching shear strength of the punching load capacity in the column–slab connection in the case in which no shear reinforcement is applied. The failure surface is assumed to be twice the slab’s depth away from the column edges and the maximum flat slab shear strength was calculated using Equation (7). The ultimate shear strength of the experimentally tested flat slab NF was calculated using Equation (7) and compared to the experimental results as shown in Table 8.

$$V_c = 0.18 k (100 \rho f_{cu})^{\frac{1}{3}} \cdot b_0 d \tag{7}$$

$$\lambda_s = 1 + \sqrt{\frac{200}{d}} \leq 2.00$$

$$\rho = \sqrt{\rho_x \cdot \rho_y} \leq 0.02$$

where λ_s is the coefficient of size effect; b_0 is the perimeter of the critical section; f_{cu} is the concrete characteristic compressive strength and does not exceed 80 MPa; and V_c is the ultimate punching load capacity.

6.4.2. Post-Tensioned Reinforced Concrete Flat Slab

The Euro code considers the effect of the prestressing force as enhancement of the punching shear strength only if it locates at a distance of six times the column diameter away from the column edges; this is known as the basic control area, according to the proposed design code. Additionally, the euro code takes the effect of the prestressing as the addition of the vertical component of the inclined tendons to the basic control zone only, as shown in Equation (8). The ultimate shear strength of the experimentally tested flat slabs C2PS, C3PS, D2PS, D3PS were calculated using Equation (8) and compared to the experimental results, as shown in Table 8.

$$V_c = (0.18 \lambda_s (100 \rho f_{cu})^{\frac{1}{3}} + k_1 \cdot \sigma_{cp}) \cdot b_0 d \tag{8}$$

$$\sigma_{cp} = \frac{\sigma_{cy} + \sigma_{cz}}{2}$$

$$\sigma_{cy} = \frac{N_{Ed,y}}{A_{cy}} \text{ and } \sigma_{cz} = \frac{N_{Ed,z}}{A_{cz}}$$

where λ_s is the coefficient of size effect; $\sigma_{Ed,y}$ and $\sigma_{Ed,z}$ are the normal concrete stresses in the critical section in y- and z directions, respectively (MPa, positive if compression); and $N_{Ed,y}$ and $N_{Ed,z}$ are the longitudinal forces across the full bay for internal columns and the longitudinal force across the control section for edge columns, respectively. The force may be from a load or prestressing action; k_1 : 0.1.

7. Conclusions

In this paper, an experimental study was conducted to investigate the effect of various parameters on the punching shear behavior of flat slabs. These parameters were the level of PT and the layout of cables around the column–slab connection. Based on the experimental results of the current study, the following conclusions can be drawn:

1. All tested flat slabs failed due to brittle punching shear, however post-tensioned flat slabs achieved a significant delay in the appearance of the first crack and crack propagation when compared with the control non-prestressed slab. The average punching cone diameter in PT flat slabs is larger than the control specimen.
2. The increase of the prestressing force is directly proportional to the punching shear strength of the slab–column connection in case of distributed post-tensioning force. As flat slabs with distributed strands, D2PS and D3PS achieved punching shear strengths of 36.71% and 41.01% more than the same slabs without post-tensioning, respectively. While the slab–column connections with banded strands C2PS and C3PS recorded shear strengths 64.56% and 48.35%, respectively, when compared to slabs with no prestressing in cases of banded and distributed prestressing level. This clearly shows that the banded lay out of the post-tensioning strands enhanced the punching shear strength in different PT levels.
3. Increase of PT level significantly decreased the deflection at ultimate load. Additionally, distributed lay out of strands delayed the punching shear failure. This is demonstrated by the way that the deflections at ultimate load of flat slabs were decreased by 17.11%, 45.5%, 14.97% and 22.5% in case of C2PS, C3PS, D2PS and D3PS, respectively, when compared to the control flat slab NF.
4. Ductility (μ) of a flat slab is significantly influenced by the level of post-tensioning, as the ductility decreased by 10.05% and 8.995%, respectively, in cases of low post-tensioning level and decreased by 11.64% and 21.69%, respectively, for slabs of higher prestressing level in cases of banded and distributed strands, when compared with non-prestressed slabs.
5. Ductility of flat slabs is highly affected by the distribution of the strands in case of high prestressing force. Ductility decreased by 8.995% and 21.69% for slabs with distributed strands with a higher level of PT. However, the effect of the distribution of the PT force decreases in cases of low PT force, as the ductility decreased by 10.05% and 11.64% in cases of banded and distributed strands, respectively.
6. The absorbed energy index (AEI) is inversely proportional to the PT level. The flat slabs with low level of prestressing achieved AEI 19.6 and 10.955 in the cases of banded and distributed strands, respectively. Meanwhile, the flat slabs with high level of prestressing achieved AEI 7.15 and 10.35 in the cases of banded and distributed strands, respectively.
7. Calculation of ultimate punching shear strength based on equations provided by different design codes are comparable to the experimental test results. The Egyptian code of practice gives very conservative ultimate punching shear strength in both cases of non-prestressed and prestressed flat slabs. Predicted values using the ACI are remarkably close to the experimental results, but the error increases with an increase in the distribution and an increase in the post-tensioning force. CEB values are consistent with the measured flat slab strength. The Euro code came the closest to predicting the correct ultimate punching shear strength of post-tensioned flat slabs, with no conservative prediction.

Author Contributions: Conceptualization, A.K.S.; Supervision, A.K.S.; Formal Analysis, S.S.E. and D.M.O.; Investigation, S.S.E.; Resources, A.H.; visualization, S.S.E.; Writing—Review and Editing, A.H.; Validation, A.K.S.; Project Administration, D.M.O.; Writing original draft D.M.O. All authors have read and agreed to the published version of the manuscript.

Funding: This research received no external funding.

Institutional Review Board Statement: Not applicable.

Informed Consent Statement: Not applicable.

Data Availability Statement: The data presented in this study are provided through the current manuscript.

Conflicts of Interest: The authors declare no conflict of interest regarding this work’s intellectual and commercial property.

Notations

a, b	short and long dimensions of column dimensions
b_0	perimeter of critical section of punching
d	slab thickness
f'_c	concrete cylinder compressive strength
f_{cu}	concrete characteristic compressive strength
f_{pc}	the mean effective prestress
PT	Post-tensioned
V_c	ultimate punching load capacity
V_p	the vertical component of prestress in tendon at supports
λ_s	size effect factor
β_c	column aspect ratio (long side/short side)

References

- Malvade, S.S.; Salunke, P. Analysis of Post-Tensioned Flat Slab by using SAFE. *Int. J. Sci. Eng. Appl. Sci. (IJSEAS)* **2017**, *3*, 92–95.
- Mohammed, A.H.; Tayşi, N.; Nassani, D.E.; Hussein, A.K. Finite element analysis and optimization of bonded post-tensioned concrete slabs. *Cogent Eng.* **2017**, *4*, 1341288. [[CrossRef](#)]
- Abd-El-Mottaleb, H.E.; Mohamed, H.A. Behaviour of Two-Way Post Tension Flat Slab. *Appl. Eng. Sci.* **2018**, *2*, 54–59. [[CrossRef](#)]
- Puskás, A.; Töröka, I.; Virág, J. Price comparison of three post-tensioned flat slabs beside classic flat slabs from three existing structures/under construction. In Proceedings of the 12th PhD Symposium, Prague, Czech Republic, 29–31 August 2018.
- Töröka, I.; Puskás, A.; Virág, J. Post-tensioned Flat Slabs with Unbonded Tendons for Public Buildings. *Procedia Manuf.* **2019**, *32*, 102–109. [[CrossRef](#)]
- Luu, B.T.; Ngo-Huu, C.; Nguyen-Minh, L. Punching shear capacity of unbonded post-tensioned slab-Concrete filled steel tube column joints with innovative connections: Experiment and A new prediction model. *J. Build. Eng.* **2022**, *59*, 104974. [[CrossRef](#)]
- Eid, H.; Riad, K.H.; Zaher, A.H. Punching Shear Strength of Pre-Stressed Flat Slab in Case of Near-Column Openings. *World Appl. Sci. J.* **2014**, *32*, 780–791. [[CrossRef](#)]
- Husain, M.; Eisa, A.S.; Roshdy, R. Alternatives to Enhance Flat Slab Ductility. *Int. J. Concr. Struct. Mater.* **2017**, *11*, 161–169. [[CrossRef](#)]
- Egyptian Code for Design and Construction of Reinforced Concrete Structures, ECPCS-203*; Housing and Building National Research Center, Ministry of Housing, Utilities and Urban Planning: Cairo, Egypt, 2018.
- ACI Committee 318. *Building Code Requirements for Structural Concrete and Commentary, ACI 318M-08*; American Concrete Institute: Michigan, MI, USA, 2008.
- CEB-FIP MC90 *Model Code, Model Code for Concrete Structures*; Comintary International du Baton et Federation International de la Precontrainte: Lausanne, Switzerland, 1990.
- Part 1-1: General Rules and Rules for Buildings. In *Design of Concrete Structures; Eurocode2*; British Standards Institution: Brussels, Belgium, 2004.

Disclaimer/Publisher’s Note: The statements, opinions and data contained in all publications are solely those of the individual author(s) and contributor(s) and not of MDPI and/or the editor(s). MDPI and/or the editor(s) disclaim responsibility for any injury to people or property resulting from any ideas, methods, instructions or products referred to in the content.